# Thermochemistry and kinetics of the *trans-N$_2$H$_2$ + N* reaction

Rene F.K. Spada [a,b], Luiz F.A. Ferrão [a,b], Daniely V.V. Cardoso [a], Orlando Roberto-Neto [c], Francisco B.C. Machado [a,*]

[a] *Departamento de Química, Instituto Tecnológico de Aeronáutica, São José dos Campos, 12.228-900 São Paulo, Brazil*
[b] *Departamento de Física, Instituto Tecnológico de Aeronáutica, São José dos Campos, 12.228-900 São Paulo, Brazil*
[c] *Divisão de Aerotermodinâmica e Hipersônica, Instituto de Estudos Avançados, São José dos Campos, 12.228-001 São Paulo, Brazil*

## ARTICLE INFO

## ABSTRACT

Thermochemical and kinetics properties of the hydrogen abstraction and addition processes of the *trans-N$_2$H$_2$ + N* reaction were computed using high-level *ab initio* and DFT approximation methods with aug-cc-pVXZ (X = T,Q) basis set. The CCSD (T)/CBS//BB1K/aug-cc-pVTZ results for classical barrier height are 13.1 and 15.0 kcal/mol for the abstraction and addition reactions, respectively. The thermal rate constants were calculated using the dual-level direct dynamics by variational transition state theory with the BB1K potential energy surface and thermochemical properties corrected with the CCSD (T)/CBS//BB1K/aug-cc-pVTZ results. The rate constants calculated show that the variational and tunneling effects play a relevant role only for the abstraction reaction.

© 2012 Elsevier B.V. All rights reserved.

## 1. Introduction

Reactions involving $N_2H_X$ kind of molecules are of great importance since they are present in several chemical kinetics mechanisms proposed to describe the chemistry of diamine based propellants. One of these molecules, the diazene ($N_2H_2$), is involved in several elementary reactions of the kinetic mechanism proposed for the hydrazine ($N_2H_4$) decomposition [1], which is a propellant widely used in attitude control system of spacecrafts [2] over a wide range of conditions [3,4]. Concerning the hydrazine molecule, the vibrational frequencies, equilibrium geometry and the ionization potential were investigated by our group in previous works [5,6].

It is well known that, in most of kinetics mechanisms proposed in the literature for the hydrazine decomposition, the elementary reaction rate constants are estimated, only a few are measured. Besides its importance in elementary steps of the hydrazine decomposition, the reactions involving diazene are also fundamental in the pyrolysis of ammonia [7]. Among other elementary reactions of these mechanisms, the ones involving $N_2H_2$ with radicals, like $H$ and $N$, are fundamental steps. To our knowledge, there are no experimental data for these reactions, however, the diazene reaction with the hydrogen atom was theoretically well characterized [8,9]. The main goal of this Letter is to determine the barrier heights and the reaction rates for the *trans-N$_2$H$_2$ + N* reaction system.

In the transition state theory (TST) model [10–12], accurate evaluation of the classical barrier height and the structures of stationary points (reactants, transition state (TS) and products) are generally the main factors in order to obtain reliable thermal rate constants of chemical reactions. The strategies to calculate these thermochemical properties are discussed in some selected works in the literature [13–15]. The TST assumes that the TS is located at the saddle point (SP), and to obtain better results, it is important to use the canonical variational transition state theory (CVT), which uses information of non-stationary points along the potential energy surface to maximize the Gibbs free energy and find more reliable transition states, leading to more accurate rate constants [11,12].

In this Letter two reaction paths of the *trans-N$_2$H$_2$ + N* system were studied, the hydrogen abstraction (R1), *trans-N$_2$H$_2$ + N* → $N_2H + NH$, and the addition (R2), *trans-N$_2$H$_2$ + N* → $N_3H_2$, both represented in Figure 1. In the CVT rate constants calculations, the potential energy surfaces were generated using the BB1K functional, and the properties of the stationary points were corrected by a highly correlated method, CCSD (T) at the BB1K optimized geometry. This procedure is known as dual-level methodology [16].

## 2. Methodology

The calculations were carried out using *ab initio* methods, such as second order Møller–Plesset (MP2) [17] and coupled cluster with single, double and quasi-perturbative triple excitations (CCSD (T)) [18]. These methodologies use only one Slater determinant (configuration) reference and are known as single reference (SR) wave function methods. However, it is well known that one should figure

* Corresponding author.

*E-mail addresses:* rfkspada@gmail.com (R.F.K. Spada), ferrao_lfa@yahoo.com.br (L.F.A. Ferrão), daniely@ita.br (D.V.V. Cardoso), orlando@ieav.cta.br (O. Roberto-Neto), fmachado@ita.br (F.B.C. Machado).
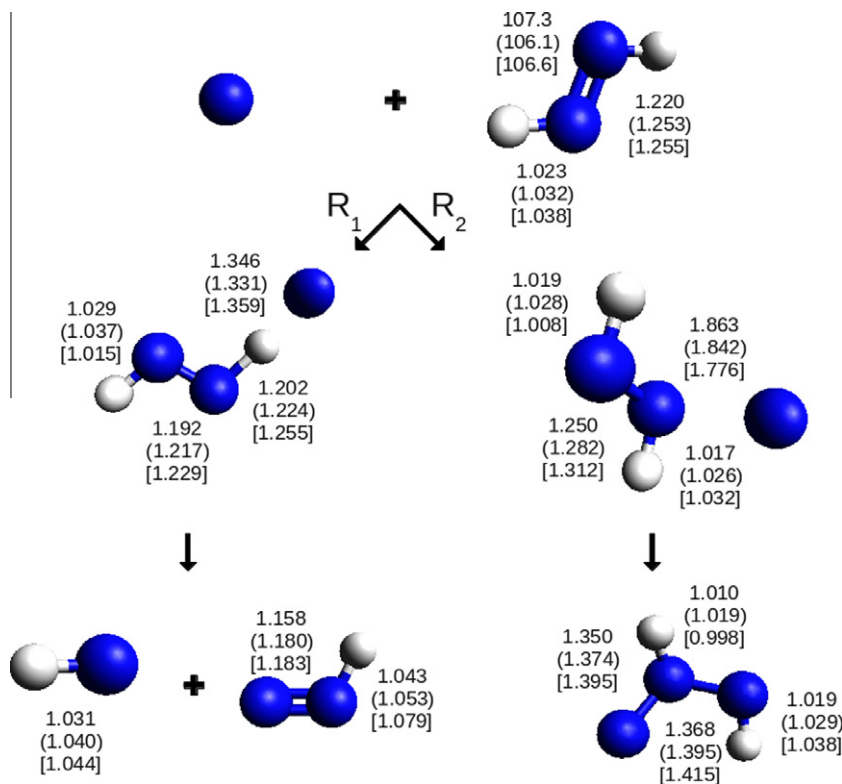
**Figure 1.** The hydrogen abstraction (R1) and addition (R2) reaction paths for the $N_2H_2 + N$ system. The bond distances (Å) stands for BB1K/aTZ (firts line), CCSD (T)/aTZ (second line, in parenthesis) and CASSCF (third line, in brackets).

out other configurations contribution to the wave function. One can use the $T_1$ diagnostic [19], which takes in account the single excitations on the CCSD method to estimate the multireference (MR) character of the system. According to Lee and Taylor [19], a value of $T_1$ diagnostic greater than 0.02 indicates a certain multiconfiguration character, although Rienstra–Kiracofe et al. have argued that it become significant with values greater than 0.044 [20].

The MR methods were also employed in the present work, starting with the geometry optimization and the harmonic frequencies calculation of all stationary points using the complete active space self-consistent field (CASSCF) [21]. The CASSCF active space contains all valence electrons and orbitals, that is, 17 electrons in 14 orbitals. Using these geometries and orbitals, single-point calculations were performed using MR second order perturbation theory (CASPT2) [22] and internally contracted MR configuration interaction theory with single and double excitations (MRCI) [23], also including the Davidson's correction to the energy (MRCI + Q) [24]. However, these calculations were carried out using a smaller reference set, the one built with an active space of 11 electrons in 11 orbitals. Using the CASSCF calculations, the multireference character of the wave functions were also estimated by the use of M diagnostic [25], which takes in account the occupancy number of the natural orbitals in the CASSCF calculations. The value of M diagnostic smaller than 0.05, in the interval of 0.05–0.1, and greater than 0.1 are considered to present a low, moderate and high multireference character in the wave function, respectively [25].

The optimization of geometries and frequencies of the stationary points were also calculated using density functional theory (DFT) approximations. The functionals employed were B3LYP [26,27] and the hybrid meta-GGA BB1K [28], M05 [29], M05-2X [30], M06, M06-2X [31] and M06L [32].

All of the electronic calculations were performed with the aug-cc-pVXZ (X = T,Q) basis set [33], which will be abreviated to aXZ (X = T,Q) along the text.

The intrinsic reaction coordinate (IRC) [34,35] calculations were carried out to verify the connection between transition states and equilibrium geometries of the reactants and products.

The reactions energetic properties were also performed using CCSD (T) single point calculations at the BB1K/aTZ geometries and frequencies, which can be compared with the results obtained at the CCSD (T) optimized equilibrium geometries. In the CCSD (T) and MRCI calculations, we used the aXZ (X = T,Q) basis set and energetic properties were extrapolated to the complete basis set (CBS) limit using the extrapolation procedure of Halkier et al. [36],

$$E_{CBS} = \frac{\left[ E(n) \times n^3 - E(n-1) \times (n-1)^3 \right]}{\left[ n^3 - (n-1)^3 \right]}, \tag{1}$$

where $n$ is equal to 4 for the aQZ basis set.

The calculated energetic properties are the classical barrier height ($V^\ddagger$) (defined as the electronic energy difference between the transition state and the reactants), the vibrationally adiabatic barrier height (evaluated at the transition state for the forward reaction ($\Delta V_a^{G,\ddagger}$) and defined as $V^\ddagger + \Delta ZPE$), the electronic energy of reaction ($\Delta E$), and the enthalpy of the reaction at 0 K ($\Delta H_0^o$).

For reactions R1 and R2, the thermal rate constants were calculated using dual-level direct dynamics, in particular by variational transition state theory with interpolated single-point-energy corrections (VTST-ISPE) [16]. This approach involves the simultaneous use of two levels of calculations. At a lower-level BB1K/aTZ was used in the calculation of the potential energy surface, generating gradients and Hessians for the whole reaction path. As discussed below, the BB1K functional presented the best DFT results compared to the high-level *ab initio* methods. For the high-level, the classical barrier heights and reaction energies were calculated using the CCSD (T)/CBS//BB1K/aTZ method. In the canonical variational transition state (CVT) calculations, we also included

the tunneling effects using the zero-curvature tunneling (CVT/ZCT) [37,38] and small-curvature tunneling (CVT/SCT) [39] methods.

The calculations were performed using the Gaussian 09 [40] and MOLPRO 2010.1 [41] computational packages for the single-reference and multireference electronic structure methods, respectively. The chemical kinetics was calculated using the Polyrate package [42] and the Gaussrate interface [43] (an interface between Polyrate and Gaussian packages), for the potential energy surface calculations.

## 3. Results and discussion

The geometries of saddle point, reactants and products for the $N_2H_2 + N \rightarrow N_2H + NH$ (R1) and $N_2H_2 + N \rightarrow N_3H_2$ (R2) reaction paths were optimized using DFT approximations, CASSCF, MP2 and the CCSD (T) levels of theory.

Figure 1 shows the structures of all of the stationary points (reactants, products, and saddle-point) of reactions R1 and R2 with selected key values of bond distances and angles optimized using the CCSD (T) [18], CASSCF [21] and BB1K [28] methods with the aTZ basis set [33]. The vibrational harmonic frequencies calculated at the same levels are listed in Table 1. The complete set of geometrical parameters and vibrational frequencies is available by request.

The calculated equilibrium geometries of $N_2H_2$ and $NH$ can be compared with their experimental data. For $N_2H_2$, the experimental values [44] of distances $N - H, N - N$ and the angle HNN are 1.029 Å, 1.247 Å, and 106.3°, respectively, and for $NH$, the experimental distance is 1.0362 Å [45]. Our best results calculated at CCSD (T)/CBS, are equal to 1.029 Å, 1.246 Å, and 106.4° for the geometry parameters of $N_2H_2$, and equal to 1.036 Å for the NH distance, which are in excellent agreement with the experimental results. Note also that the CCSD (T)/aTZ and BB1K/aTZ results are close and in good agreement with the experimental data. Due to the high exoergicity of the reaction R1, and in accord with the Hammond's postulate [46], the extention of the formation $N-H$ is larger than that of the breaking $N-H$ bond, as shown in the transition state structure of Figure 1. Also, the R2 reaction has an early transition state, in which the geometry of $N_2H_2$ moiety does not present significant changes (Figure 1). The same behavior occurs for the two similar reactions in the $N_2H_2 + H$ reaction system [8]. Note also that, for the two reactions, the BB1K/aTZ and CCSD (T)/aTZ transition states geometries are in good agreement.

For the transition states, the vibrational analysis demonstrates that their respective modes correspond to the expected reaction paths and all saddle-points have only one imaginary frequency. Accurate calculations of vibrational modes, mainly their imaginary frequency, are very important in modeling the global potential of surfaces for dynamical calculations [47], and we have shown previously [48,49] that the BB1K functional produces imaginary frequencies for the transition states that are in good agreement with the CCSD (T) calculations, as obtained for the present reactions.

Tables 2 and 3 include the calculated electronic barrier heights with and without the zero-point energies, electronic reaction energies, and enthalpies of reaction at 0 K of the two reaction paths of the $N(^4S) + trans$-$N_2H_2$ reactions. The best estimates of the energetic properties were calculated using both single-reference (SR) and multireference (MR) methods. Before discussing these results, we first attempt to quantify the multireference character in the electronic wave functions by using the $T_1$ and M diagnostics.

The $T_1$ diagnostic computed for $N_2H_2$ (0.012), $N_2H$ (0.044), $SP_{R1}$ (0.045), $NH$ (0.011), $N$ (0.007), $SP_{R2}$ (0.043) and $N_3H_2$ (0.023) indicates that $N_2H, SP_{R1}$ and $SP_{R2}$ have a certain multireference character, although they are in the limit which can be treated by single-reference methods. The calculated M diagnostic for $N_2H_2, N_2H, SP_{R1}$, $NH, SP_{R2}$ and $N_3H_2$ are 0.086, 0.083, 0.074, 0.028, 0.120 and 0.047, respectively. As affirmed before, values of M between 0.05 and 0.10 and greater than 0.1 are considered to have a modest and large character. Although these results confirm the non-negligible multireference character in $N_2H, SP_{R1}$, and $SP_{R2}$, the single-reference CCSD (T) wave function can be considerate a reliable model to treat these two reaction paths, as discussed below.

For the R1 reaction path, our best results based on single-reference method for classical barrier height ($V^\ddagger$) and electronic energy of reaction ($\Delta E$) are those calculated using CCSD (T)/CBS, equal to 13.1 and $-10.8$ kcal/mol, respectively. The results obtained using the single point CCSD (T)/CBS//BB1K/aTZ, respectively equal to 13.1 and $-11.0$ kcal/mol are practically equal to the CCSD (T)/CBS results. The calculated values for the vibrationally adiabatic barrier height ($\Delta V_a^{G,\ddagger}$) using CCSD (T)/CBS (9.8 kcal/mol) and using the single point CCSD (T)/CBS//BB1K/aTZ (9.4 kcal/mol), differs by only 0.4 kcal/mol. This indicates that the zero point energies calculated with the BB1K/aTZ and CCSD (T)/CBS are in good agreement. Note also that the best results calculated with the density functional theory approximations are those obtained with the BB1K functional. Using the multireference methods, our best results for the classical barrier height ($V^\ddagger$) and the electronic energy of reaction ($\Delta E$) are respectively equal to 17.5 and $-11.9$ kcal/mol at the single

**Table 1**
Harmonic vibrational frequencies (cm$^{-1}$) for the reatctants, saddle-points and products calculated using BB1K (first line), CCSD (T) (second line) and CASSCF (third line) with aug-cc-pVTZ basis set.

| Molecule | Frequencies | | | | | | | | |
|---|---|---|---|---|---|---|---|---|---|
| $N_2H_2$ | 3392 | 3358 | 1751 | 1629 | 1378 | 1376 | | | |
| | 3297 | 3265 | 1611 | 1552 | 1344 | 1317 | | | |
| | 3158 | 3124 | 1617 | 1527 | 1354 | 1321 | | | |
| $N_2H$ | 2977 | 1968 | 1130 | | | | | | |
| | 2880 | 1848 | 1108 | | | | | | |
| | 2424 | 1712 | 1120 | | | | | | |
| $NH$ | 3366 | | | | | | | | |
| | 3264 | | | | | | | | |
| | 3150 | | | | | | | | |
| $N_3H_2$ | 3546 | 3484 | 1520 | 1336 | 1155 | 1112 | 865 | 528 | 419 |
| | 3454 | 3367 | 1491 | 1308 | 1081 | 1027 | 860 | 527 | 418 |
| | 3744 | 3258 | 1544 | 1349 | 1048 | 998 | 870 | 513 | 430 |
| $SP_{R1}$ | 3283 | 1830 | 1427 | 1287 | 1234 | 587 | 475 | 184 | 2113i |
| | 3207 | 1701 | 1394 | 1263 | 1204 | 576 | 460 | 168 | 2441i |
| | 3547 | 1623 | 1440 | 1269 | 1193 | 521 | 478 | 160 | 2916i |
| $SP_{R2}$ | 3466 | 3431 | 1547 | 1434 | 1329 | 1195 | 567 | 334 | 607i |
| | 3365 | 3329 | 1523 | 1320 | 1294 | 1151 | 558 | 330 | 685i |
| | 3628 | 3305 | 1578 | 1337 | 1204 | 1117 | 599 | 366 | 846i |

**Table 2**
Thermochemistry of the R1 reaction path ($trans$-$N_2H_2$ + N → $N_2H$ + NH). Values are in kcal/mol.

| Method | $\Delta E$ | $\Delta H$ | $V^\ddagger$ | $\Delta V_a^{G,\ddagger}$ |
|---|---|---|---|---|
| MP2/aTZ | −2.4 | −5.6 | 23.3 | 22.3 |
| BB1K/aTZ | −12.7 | −17.6 | 10.3 | 6.6 |
| M05/aTZ | −14.8 | −19.9 | 6.3 | 2.7 |
| M06/aTZ | −12.3 | −17.5 | 6.5 | 3.1 |
| M06L/aTZ | −15.0 | −19.9 | 1.7 | −1.5 |
| M05-2X/aTZ | −13.9 | −18.7 | 8.8 | 5.0 |
| M06-2X/aTZ | −12.9 | −17.8 | 7.4 | 3.7 |
| B3LYP/aTZ | −19.3 | −24.1 | 2.1 | −1.0 |
| CCSD (T)/aTZ | −9.1 | −13.8 | 13.8 | 10.3 |
| CCSD (T)/aQZ | −10.1 | −14.8 | 13.4 | 10.0 |
| CCSD (T)/CBS | −10.8 | −15.5 | 13.1 | 9.8 |
| CCSD (T)/aTZ//BB1K/aTZ | −9.4 | −14.3 | 13.5 | 9.8 |
| CCSD (T)/aQZ//BB1K/aTZ | −10.3 | −15.2 | 13.3 | 9.6 |
| CCSD (T)/CBS//BB1K/aTZ | −11.0 | −15.9 | 13.1 | 9.4 |
| MRCI/aTZ//CASSCF/aTZ | −9.0 | −14.3 | 28.0 | 25.3 |
| MRCI/aQZ//CASSCF/aQZ | −9.9 | −15.3 | 30.9 | 27.1 |
| MRCI/CBS//CASSCF/a (T/Q) Z | −10.6 | −16.0 | 33.0 | 28.4 |
| MRCI + Q/aTZ//CASSCF/aTZ | −10.3 | −15.6 | 15.4 | 12.8 |
| MRCI + Q/aQZ//CASSCF/aQZ | −11.2 | −16.7 | 16.6 | 12.7 |
| MRCI + Q/CBS//CASSCF/a (T/Q) Z | −11.9 | −17.5 | 17.5 | 12.6 |
| CASPT2/aTZ//CASSCF/aTZ | −10.8 | −16.1 | 11.6 | 9.0 |
| CASPT2/aQZ//CASSCF/aQZ | −11.9 | −17.2 | 11.2 | 8.5 |
| CASPT2/CBS//CASSCF/a (T/Q) Z | −12.7 | −18.0 | 10.9 | 8.1 |

**Table 3**
Thermochemistry of the R2 reaction path ($trans$-$N_2H_2$ + N → $N_3H_2$). Values are in kcal/mol.

| Method | $\Delta E$ | $\Delta H$ | $V^\ddagger$ | $\Delta V_a^{G,\ddagger}$ |
|---|---|---|---|---|
| MP2/aTZ | 1.0 | 3.0 | 30.7 | 31.8 |
| BB1K/aTZ | −12.0 | −10.4 | 12.7 | 13.3 |
| M05/aTZ | −14.1 | −12.5 | 8.9 | 9.6 |
| M06/aTZ | −11.1 | −9.5 | 10.3 | 10.9 |
| M06L/aTZ | −14.1 | −12.5 | 5.9 | 6.5 |
| M05-2X/aTZ | −13.6 | −12.2 | 10.6 | 11.1 |
| M06-2X/aTZ | −11.1 | −9.7 | 10.7 | 11.2 |
| B3LYP/aTZ | −16.7 | −15.3 | 6.2 | 6.9 |
| CCSD (T)/aTZ | −3.5 | −1.8 | 16.0 | 16.7 |
| CCSD (T)/aTZ//BB1K/aTZ | −3.7 | −2.2 | 15.5 | 16.1 |
| CCSD (T)/aQZ//BB1K/aTZ | −5.3 | −3.8 | 15.2 | 15.8 |
| CCSD (T)/CBS//BB1K/aTZ | −6.5 | −5.0 | 15.0 | 15.6 |

point MRCI + Q/CBS, and equal to 10.9 and −12.7 kcal/mol at the single point CASPT2/CBS. Note that the classical barrier height calculated by CCSD (T)/CBS//BB1K/aTZ is 2.2 kcal/mol lower than the multireference CASPT2/CBS. The MRCI + Q/CBS predicted a value which seems to be too high, and it is also very different from the value obtained without the Davidson correction, equal to 33.0 kcal/mol. For the $\Delta E$, the single reference and multireference results differ no more than 3.3 kcal/mol. Therefore, the CCSD (T)/CBS//BB1K/aTZ results can be considered reliable to this reaction path and it was used as the high-level method in the calculations of R1 and R2 reaction paths.

For the R2 reaction path, as discussed before, our best results are based only on single-reference methods. The CCSD (T)/CBS//BB1K/aTZ calculated values for classical barrier height ($V^\ddagger$) and electronic energy of reaction ($\Delta E$) are equal to 15.0 and −6.5 kcal/mol, respectively. Compared to this results, we also found that, between the DFT methods, the BB1K functional present the best results followed by M06−2X. The vibrationally adiabatic barrier height ($\Delta V_a^{G,\ddagger}$) for this reaction, equal to 15.6 kcal/mol, is 6.2 kcal/mol higher than that for the reaction R1, indicating that R1 is the most important path.

In the calculation of the rate constants, the potential energy surfaces were generated using BB1K/aTZ within curvilinear
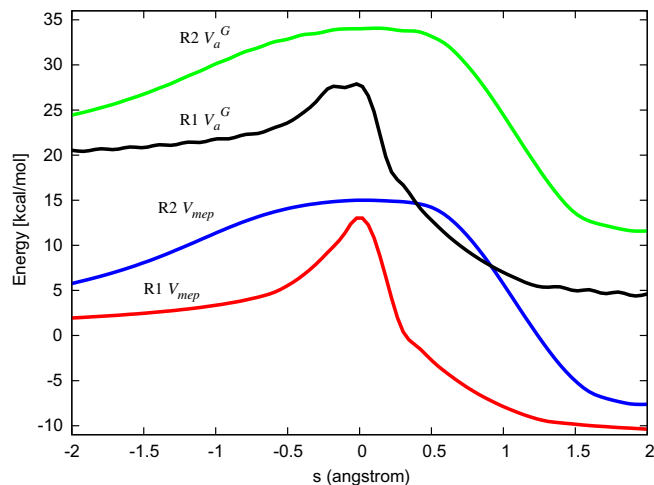


**Figure 2.** Minimum energy curve ($V_{mep}$) and vibrationally adiabatic potential curve ($V_a^G$) of R1 and R2 calculated by the BB1K/aTZ method and corrected with the CCSD (T)/CBS//BB1K/aTZ thermochemistry results.

**Table 4**
Rate constants (in cm³ mol⁻¹ s⁻¹) for the R1 reaction path ($trans$-$N_2H_2$ + N → $N_2H$ + NH).[a]

| T (K) | TST | CVT | CVT/ZCT | CVT/SCT |
|---|---|---|---|---|
| 200 | 2.66E−22 | 1.83E−22 | 1.05E−20 | 7.30E−20 |
| 250 | 3.23E−20 | 2.39E−20 | 2.30E−19 | 1.10E−18 |
| 298 | 7.44E−19 | 5.75E−19 | 2.40E−18 | 8.17E−18 |
| 300 | 8.30E−19 | 6.43E−19 | 2.61E−18 | 8.79E−18 |
| 350 | 8.79E−18 | 7.01E−18 | 1.81E−17 | 4.60E−17 |
| 400 | 5.34E−17 | 4.35E−17 | 8.58E−17 | 1.78E−16 |
| 500 | 7.21E−16 | 6.01E−16 | 8.93E−16 | 1.43E−15 |
| 600 | 4.41E−15 | 3.71E−15 | 4.78E−15 | 6.64E−15 |
| 700 | 1.70E−14 | 1.44E−14 | 1.70E−14 | 2.16E−14 |
| 800 | 4.90E−14 | 4.13E−14 | 4.62E−14 | 5.55E−14 |
| 900 | 1.15E−13 | 9.65E−14 | 1.04E−13 | 1.20E−13 |
| 1000 | 2.35E−13 | 2.13E−13 | 2.24E−13 | 2.52E−13 |
| 1100 | 4.29E−13 | 3.82E−13 | 3.85E−13 | 4.23E−13 |
| 1200 | 7.22E−13 | 6.27E−13 | 6.09E−13 | 6.61E−13 |
| 1300 | 1.14E−12 | 9.65E−13 | 9.09E−13 | 9.74E−13 |
| 1400 | 1.70E−12 | 1.41E−12 | 1.30E−12 | 1.38E−12 |
| 1500 | 2.43E−12 | 1.96E−12 | 1.80E−12 | 1.89E−12 |
| 1600 | 3.35E−12 | 2.64E−12 | 2.41E−12 | 2.52E−12 |
| 1700 | 4.49E−12 | 3.45E−12 | 3.16E−12 | 3.29E−12 |
| 1800 | 5.86E−12 | 4.40E−12 | 4.04E−12 | 4.19E−12 |
| 1900 | 7.47E−12 | 5.50E−12 | 5.07E−12 | 5.24E−12 |
| 2000 | 9.35E−12 | 6.74E−12 | 6.25E−12 | 6.43E−12 |
| 2100 | 1.15E−11 | 8.14E−12 | 7.57E−12 | 7.78E−12 |
| 2200 | 1.40E−11 | 9.69E−12 | 9.06E−12 | 9.27E−12 |
| 2300 | 1.67E−11 | 1.14E−11 | 1.07E−11 | 1.09E−11 |
| 2400 | 1.98E−11 | 1.33E−11 | 1.25E−11 | 1.27E−11 |
| 2500 | 2.31E−11 | 1.53E−11 | 1.44E−11 | 1.47E−11 |
| 2600 | 2.68E−11 | 1.75E−11 | 1.66E−11 | 1.68E−11 |
| 2700 | 3.08E−11 | 1.99E−11 | 1.88E−11 | 1.91E−11 |
| 2800 | 3.52E−11 | 2.24E−11 | 2.13E−11 | 2.16E−11 |
| 2900 | 3.99E−11 | 2.51E−11 | 2.39E−11 | 2.42E−11 |
| 3000 | 4.49E−11 | 2.79E−11 | 2.66E−11 | 2.70E−11 |

[a] The E stands for powers of ten.

coordinates, updating the gradient every 0.02 Å and the Hessian matrix each 0.1 Å. Also the energies of the stationary points were corrected with the CCSD (T)/CBS//BB1K/aTZ values. The potential energy surface are presented in Figure 2. The symmetry number of the reactions were calculated using the rotational symmetry numbers ($\sigma_f$) of the point-group symmetries, according to Fernández–Ramos et al. [50]. The reactants present symmetry $C_s$ for the $N_2H_2$ and $C_{\infty v}$ for the nitrogen atom. The saddle points of R1 and R2 paths have $C_s$ and $C_1$ symmetries, respectively, and the $\sigma_f$ is equal to 1 for both reaction paths. However, the SP of the addition

**Table 5**
Rate constants (in $cm^3 \, mol^{-1} \, s^{-1}$) for the R2 reaction path ($trans\text{-}N_2H_2 + N \rightarrow N_3H_2$).[a]

| T (K) | TST | CVT | CVT/ZCT | CVT/SCT |
|---|---|---|---|---|
| 200 | 5.38E−29 | 5.32E−29 | 6.66E−29 | 7.60E−29 |
| 250 | 1.34E−25 | 1.31E−25 | 1.50E−25 | 1.63E−25 |
| 298 | 2.12E−23 | 2.06E−23 | 2.24E−23 | 2.38E−23 |
| 300 | 2.54E−23 | 2.44E−23 | 2.68E−23 | 2.84E−23 |
| 350 | 1.10E−21 | 1.05E−21 | 1.17E−21 | 1.17E−21 |
| 400 | 1.89E−20 | 1.80E−20 | 1.88E−20 | 1.94E−20 |
| 500 | 1.06E−18 | 1.01E−18 | 1.03E−18 | 1.05E−18 |
| 600 | 1.64E−17 | 1.55E−17 | 1.56E−17 | 1.59E−17 |
| 700 | 1.21E−16 | 1.13E−16 | 1.13E−16 | 1.14E−16 |
| 800 | 5.54E−16 | 5.20E−16 | 5.04E−16 | 5.08E−16 |
| 900 | 1.85E−15 | 1.72E−15 | 1.59E−15 | 1.60E−15 |
| 1000 | 4.96E−15 | 4.52E−15 | 4.14E−15 | 4.16E−15 |
| 1100 | 1.13E−14 | 1.01E−14 | 9.26E−15 | 9.30E−15 |
| 1200 | 2.26E−14 | 2.00E−14 | 1.84E−14 | 1.85E−14 |
| 1300 | 4.10E−14 | 3.62E−14 | 3.32E−14 | 3.34E−14 |
| 1400 | 6.92E−14 | 6.04E−14 | 5.58E−14 | 5.60E−14 |
| 1500 | 1.10E−13 | 9.48E−14 | 8.80E−14 | 8.82E−14 |
| 1600 | 1.65E−13 | 1.42E−13 | 1.32E−13 | 1.32E−13 |
| 1700 | 2.38E−13 | 2.04E−13 | 1.90E−13 | 1.90E−13 |
| 1800 | 3.32E−13 | 2.82E−13 | 2.64E−13 | 2.64E−13 |
| 1900 | 4.48E−13 | 3.78E−13 | 3.56E−13 | 3.56E−13 |
| 2000 | 5.88E−13 | 4.96E−13 | 4.68E−13 | 4.68E−13 |
| 2100 | 7.58E−13 | 6.36E−13 | 6.02E−13 | 6.02E−13 |
| 2200 | 9.54E−13 | 8.00E−13 | 7.58E−13 | 7.58E−13 |
| 2300 | 1.18E−12 | 9.88E−13 | 9.38E−13 | 9.40E−13 |
| 2400 | 1.45E−12 | 1.20E−12 | 1.15E−12 | 1.15E−12 |
| 2500 | 1.74E−12 | 1.45E−12 | 1.38E−12 | 1.38E−12 |
| 2600 | 2.08E−12 | 1.72E−12 | 1.64E−12 | 1.64E−12 |
| 2700 | 2.44E−12 | 2.02E−12 | 1.93E−12 | 1.94E−12 |
| 2800 | 2.86E−12 | 2.36E−12 | 2.26E−12 | 2.26E−12 |
| 2900 | 3.30E−12 | 2.72E−12 | 2.60E−12 | 2.60E−12 |
| 3000 | 3.78E−12 | 3.12E−12 | 2.98E−12 | 3.00E−12 |

[a] The E stands for powers of ten.



**Figure 3.** Arrhenius plots of (a) $trans\text{-}N_2H_2 + N \rightarrow N_2H + NH$ (R1) and (b) $trans\text{-}N_2H_2 + N \rightarrow N_3H_2$ (R2).

reaction (R2) is chiral, it has two distinguishable structures which are mirror images of each other, so the R2 thermal rate constant is multiplied by two. The rate constants calculated in the temperature range of 200–3000 K using TST, CVT, CVT/ZCT and CVT/SCT are presented in Tables 4 and 5 and in Figure 3 for R1 and R2 paths.

The R1 is the most important path for this reactional system, it presents rate constants higher than R2 by a factor of $10^{10}$ at low temperatures (200 K), $10^2$ at 1500 K and $10^1$ at 3000 K.

Concerning the R1 path, the variational effect is important, in average the CVT rate constants is around 24% lower than the TST (see Table 4). The tunneling contributions play a significant role for the abstraction reaction path, mainly at low temperatures. In the CVT rate constants, the ZCT and SCT transmission coefficients at 298 K are about 4 and 14 times larger, respectively. At lower temperature, these transmission coefficients are much larger, although they rapidly decrease with the temperature, being no larger than 1.5 at 700 K. At even higher temperatures, the non-classical reflection is more important than tunneling, dominating ZCT from 1200 K and SCT from 1400 K.

In the R2 path, differing from R1, the variational and tunneling effects do not play a relevant role, as showed in Table 5 and displayed in Figure 3. Note in Figure 2 that the $\Delta V_a^{G,\ddagger}$ curve for R2 presents a larger width compared with the R1 path, which implies a smaller tunneling effect. Also, in R1 the reduced mass considered in the tunneling is much smaller than the one at the R2 path. The non-classical reflection for R2 becomes more important than both tunneling corrections above 800 K.

## 4. Conclusion

In this letter, two reactions paths of the $trans\text{-}N_2H_2 + N$ reaction system were studied using high-level wave-function methods
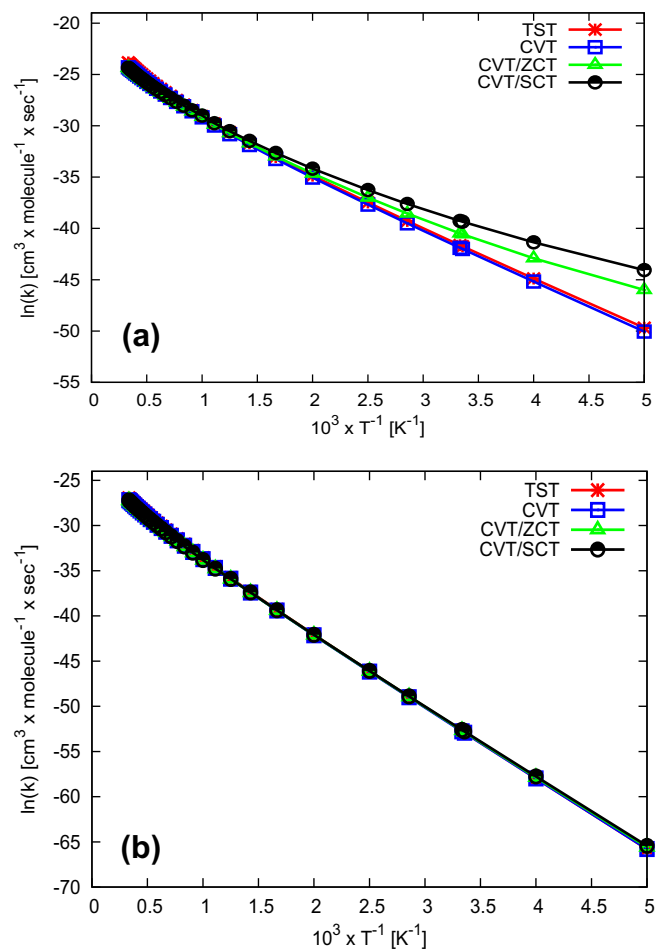
(CCSD (T), CASPT2 and MRCI) and DFT approximations. The thermochemical properties calculated using the BB1K/aTZ method presented the best results between the DFT functionals when compared to the CCSD (T) calculations.

The best estimated classical barrier height for the R1 path are in the range of 10.9 to 17.5 kcal/mol calculated at CASPT2/CBS, CCSD (T)/CBS and MRCI + Q/CBS. The rate constants were calculated using the BB1K/aTZ energy surface with the classical barrier height corrected with the CCSD (T)/CBS//BB1K/aTZ values, equal to 13.1 and 15.0 kcal/mol for the R1 and R2 reaction paths, respectively.

In this letter it was showed that the hydrogen abstraction (R1) is the most important path involved in this reaction system. Also, the variational and tunneling effects play an important role for R1, while for the addition path (R2) these effects are negligible.

## References

[1] A.A. Konnov, J. De Ruyck, Combust. Flame 124 (2001) 106.
[2] S. Ueda, Y. Kuroda, H. Miyajima, T. Kuwahara, J. Propul. Power 10 (1994) 646.
[3] M.T. Allen, R.A. Yetter, F.L. Dryer, Combust. Flame 109 (1997) 449.

[4] M.T. Allen, R.A. Yetter, F.L. Dryer, Combust. Flame 112 (1998) 302.
[5] R.J. Rocha, M. Pelegrini, O. Roberto-Neto, F.B.C. Machado, J. Mol. Struct. (THEOCHEM) 849 (2008) 98.
[6] F.B.C. Machado, O. Roberto-Neto, Chem. Phys. Lett. 352 (2002) 120.
[7] A.M. Dean, M.S. Chou, D. Stern, Int. J. Chem. Kinet. 16 (1984) 633.
[8] J. Zheng et al., J. Chem. Phys. 136 (2012) 184310.
[9] Y.Y. Chuang, E.L. Coitiño, D.G. Truhlar, J. Phys. Chem. A 104 (2000) 446.
[10] H. Eyring, J. Chem. Phys. 3 (1935) 107.
[11] D.G. Truhlar, B.C. Garrett, Acc. Chem. Res. 13 (1980) 440.
[12] D.G. Truhlar, B.C. Garrett, Annu. Rev. Phys. Chem. 35 (1984) 159.
[13] Y. Zhao, D.G. Truhlar, Chem. Phys. Lett. 502 (2011) 1.
[14] A. Karton, S. Daon, J.M.L. Martin, Chem. Phys. Lett. (2011) 165.
[15] K.A. Peterson, D. Feller, D.A. Dixon, Theor. Chem. Acc. 131 (2012) 1.
[16] Y.Y. Chuang, J.C. Corchado, D.G. Truhlar, J. Phys. Chem. A 103 (1999) 1140.
[17] J.A. Pople, J.S. Binkley, R. Seeger, Int. J. Quantum Chem. 10 (1976) 1.
[18] K. Raghavachari, G.W. Trucks, J.A. Pople, M. Head-Gordon, Chem. Phys. Lett. 157 (1989) 479.
[19] T.J. Lee, P.R. Taylor, Int. J. Quantum Chem. 36 (1989) 199.
[20] J.C. Rienstra-Kiracofe, W.D. Allen, H.F. Schaefer III, J. Phys. Chem. A 104 (2000) 9823.
[21] H.J. Werner, P.J. Knowles, J. Chem. Phys. 82 (1985) 5053.
[22] P. Celani, H.J. Werner, J. Chem. Phys. 112 (2000) 5546.
[23] H.J. Werner, P.J. Knowles, J. Chem. Phys. 89 (1988) 5803.
[24] S.R. Langhoff, E.R. Davidson, Int. J. Quantum Chem. 8 (1974) 61.
[25] O. Tishchenko, J. Zheng, D.G. Truhlar, J. Chem. Theory Comput. 4 (2008) 1208.
[26] A.D. Becke, J. Chem. Phys. 98 (1993) 5648.
[27] C. Lee, W. Yang, R.G. Parr, Phys. Rev. B 37 (1988) 785.
[28] Y. Zhao, B.J. Lynch, D.G. Truhlar, J. Phys. Chem. A 108 (2004) 2715.
[29] Y. Zhao, N.E. Schultz, D.G. Truhlar, J. Chem. Phys. 123 (2005) 161103.
[30] Y. Zhao, N.E. Schultz, D.G. Truhlar, J. Chem. Theory Comput. 2 (2006) 364.
[31] Y. Zhao, D.G. Truhlar, Theor. Chem. Acc. 120 (2008) 215.
[32] Y. Zhao, D.G. Truhlar, J. Chem. Phys. 125 (2006) 194101.
[33] T.H. Dunning Jr., J. Chem. Phys. 90 (1989) 1007.
[34] K. Fukui, J. Phys. Chem. 74 (1970) 4161.
[35] C. Gonzalez, H.B. Schlegel, J. Phys. Chem. 94 (1990) 5523.
[36] A. Halkier, T. Helgaker, P. Jorgensen, W. Klopper, H. Koch, J. Olsen, A.K. Wilson, Chem. Phys. Lett. 286 (1998) 243.
[37] B.C. Garrett, D.G. Truhlar, R.S. Grev, A.W. Magnuson, J. Phys. Chem. 84 (1980) 1730.
[38] A. Kuppermann, D.G. Truhlar, J. Am. Chem. Soc. 93 (1971) 1840.
[39] Y.P. Liu, G.C. Lynch, T.N. Truong, D.H. Lu, D.G. Truhlar, B.C. Garrett, J. Am. Chem. Soc. 115 (1993) 2408.
[40] M.J. Frisch, et al., Gaussian 09 Revision A.1, 2009. Gaussian Inc. Wallingford CT, 2009.
[41] H.J. Werner, et al., Molpro, version 2010.1, A Package of ab initio Programs, 2010.
[42] J. Zheng et al., POLYRATE, University of Minnesota, Minneapolis, 2010.
[43] J. Zheng, S. Zhang, J.C. Corchado, Y.Y. Chuang, E.L. Coitino, B.A. Ellingson, D.G. Truhlar, GAUSSRATE, University of Minnesota, Minneapolis, 2009.
[44] J. Demaison, F. Hegelund, H. Bürger, J. Mol. Struct. 413 (1997) 447.
[45] K.P. Huber, G. Herzberg, Molecular structure and molecular spectra IV: constants of diatomic molecules, Van Nostrand Reinhold Company, New York, 1979.
[46] G.S. Hammond, JACS 77 (1955) 334.
[47] T.N. Truong, D.G. Truhlar, K.K. Baldridge, M.S. Gordon, R. Steckler, J. Chem. Phys. 90 (1989) 7137.
[48] E.F.V. Carvalho, A.N. Barauna, F.B.C. Machado, O. Roberto-Neto, Chem. Phys. Lett. 463 (2008) 33.
[49] D.V.V. Cardoso, L.F.A. Ferrão, R.F.K. Spada, O. Roberto-Neto, F.B.C. Machado, Int. J. Quantum Chem. 112 (2012) 3269.
[50] A. Fernández-Ramos, B.A. Ellingson, R. Meana-Pañeda, J.M.C. Marques, D.G. Truhlar, Theor. Chem. Acc. 118 (2007) 813.